

Resolving the lithosphere–asthenosphere boundary with seismic Rayleigh waves

Stefan Bartzsch,¹ Sergei Lebedev² and Thomas Meier³

¹Friedrich Schiller Universität Jena, Faculty of Physics and Astronomy, Germany.

²Dublin Institute for Advanced Studies, School of Cosmic Physics, Geophysics Section, 5 Merrion Square, Dublin 2, Ireland. E-mail: sergei@cp.dias.ie

³Institute of Geosciences, Christian-Albrechts University of Kiel, Otto-Hahn-Platz 1, 24118 Kiel, Germany.

Accepted 2011 May 30. Received 2011 May 27; in original form 2011 March 19

SUMMARY

Seismic surface wave measurements offer tight constraints on shear wave speed values within the lithosphere and asthenosphere. It is still a matter of debate, however, how accurately and under what conditions surface waves can resolve the depth and thickness of the lithosphere–asthenosphere boundary (LAB). We investigate the sensitivity of Rayleigh waves to LAB properties and find that if the LAB is associated with a 2–3 per cent shear speed reduction at a depth less than 100 km, then 10–20 km variations in its depth translate into phase-velocity changes of up to 1 per cent. Variations in the thickness of the LAB from zero to a few tens of kilometres cause much smaller phase-velocity changes (~ 0.1 per cent), although the signal of the LAB-thickness variations is enhanced by a distinct frequency-dependent pattern of phase-velocity increases and decreases. For LAB depths increasing beyond 100 km, larger absolute variations in the LAB depth and thickness are needed to generate response of the same amplitude in phase velocities.

We introduce a grid-search inversion of phase-velocity curves for the LAB depth and thickness, defining them as the middle and the width, respectively, of a depth interval with a linear shear-speed decrease in it. The inversion comprises dense sampling of the LAB depth–LAB thickness parameter plane and non-linear, gradient-search inversions at every point; it accounts for any trade-offs of the LAB parameters with shear speed variations above and below the LAB. Inversions of phase-velocity curves for the LAB depth and thickness show that the two parameters have uncorrelated uncertainties, with the LAB depth constrained better than the LAB thickness. Random errors in phase-velocity measurements have a limited effect on LAB-depth measurements, causing errors of only a few kilometres. Measurements of the LAB thickness are less robust and are not possible in the presence of large (~ 1 per cent) random errors. Substantial systematic biases in the measurements (errors that persist over broad period ranges of tens of seconds) can affect both LAB-depth and LAB-thickness estimates; phase-velocity curves with such biases are not suitable for inversions for LAB properties. Resolving the LAB, however, in particular the LAB depth, should already be possible with some of the accurate, broad-band, phase-velocity measurements available today.

Applying our method to phase-velocity data measured in Phanerozoic west-central Germany, we find best-fitting LAB depths in the 60–80 km range (the LAB depth always understood to be the middle of the shear-speed reduction depth range), with minimum misfits achieved near the 70-km LAB depth. Beneath the Archean Guyana Shield, we determine a 140–175 km LAB-depth range, with a 160 km best-fitting (mid-)LAB depth.

Key words: Inverse theory; Surface waves and free oscillations; Seismic tomography; Computational seismology; Dynamics of lithosphere and mantle.

1 INTRODUCTION

The lithosphere and asthenosphere have distinctly different properties, and together they make up a dynamic system responsible for the fascinatingly complex patterns of tectonics and mag-

matism seen at the Earth's surface. The transition between the lithosphere and asthenosphere is central to this system, and yet its nature remains enigmatic, with available observational evidence still insufficient to capture its complexity and lateral variability.

The lithosphere is a thermal boundary layer with primarily conductive heat transfer through it; the asthenosphere is characterized by mainly advective heat transfer. The relatively stiff lithosphere makes up the tectonic plates that move coherently atop the softer asthenosphere. The lithosphere comprises the light, compositionally buoyant crust and an uppermost mantle layer that can also be compositionally distinct—mainly in its depletion in basaltic components relative to the fertile asthenosphere. It is possible, as well, that the asthenosphere, in contrast to the lithosphere, undergoes widespread partial melting, or that it contains much more water than the lithosphere (e.g. Anderson & Sammis 1970; Hirth & Kohlstedt 1996; Karato & Jung H. 1998; Hirth *et al.* 2000; Evans *et al.* 2005; Kawakatsu *et al.* 2009; Fischer *et al.* 2010).

The contrasts in the thermal, compositional and mechanical properties of the lithosphere and asthenosphere are reflected in geophysical and geological observables, including seismic-wave velocities, seismic anisotropy and attenuation, electrical conductivity and compositions of mantle-rock samples (e.g. Gaherty & Jordan 1995; Van der Lee & Nolet 1997; Gaherty *et al.* 1999; Ekström 2000, Shapiro & Ritzwoller 2002, Simons *et al.* 2002, Debayle *et al.* 2005, Evans *et al.* 2005; Fishwick *et al.* 2005, Thybo 2006, Frederiksen *et al.* 2007, Kumar *et al.* 2007, Dalton *et al.* 2008, Deschamps *et al.* 2008a, Kustowski *et al.* 2008, Darbyshire & Lebedev 2009, Lebedev *et al.* 2009, Rychert & Shearer 2009, Rychert *et al.* 2010, Tesauro *et al.* 2009, Fishwick 2010, Fullea *et al.* 2010, Jones *et al.* 2010, Kind & Yuan 2010, O'Reilly & Griffin 2010, Plomerová & Babuška 2010, Endrun *et al.* 2011). A very clear expression of the lithosphere–asthenosphere boundary (LAB) is the reduction in seismic wave speeds—from high within the colder mantle lithosphere to low within the hotter asthenosphere. The occurrence of this reduction in general is well established (e.g. Brune *et al.* 1963; Dziewonski & Anderson 1981). It has proven a challenge, however, to pinpoint either its depth or its sharpness, both of which appear to vary laterally. The LAB is deeper, for example, beneath stable ancient cratons than beneath Phanerozoic continents, but estimates of the LAB depth beneath locations of both types are debated (e.g. Eaton *et al.* 2009; Yuan & Romanowicz 2010; Fischer *et al.* 2010; Kuskov *et al.* 2011). Regarding the thickness of the LAB, the lithosphere–asthenosphere transition may well be gradual—spread over tens of kilometres—if it mirrors the typically gradual increase of temperature with depth. A sharper LAB, in contrast, could result from the presence of partial melt or water in the asthenosphere (e.g. Rychert *et al.* 2005; Kawakatsu *et al.* 2009; Fischer *et al.* 2010). Both partial melting and high water content could give rise to sharp and co-incident decreases in rock viscosity (which would define the bottom of the stiff lithospheric plate) and seismic velocities (which would facilitate the detection of the bottom of the plate).

Recently, analysis of receiver functions using broadband array data yielded abundant evidence for sharp seismic discontinuities within the lithospheric depth range. Receiver functions reveal intriguing structural complexity and appear to indicate sharp interfaces both within and at the bottom of the mantle lithosphere (Farra & Vinnik 2000; Rychert *et al.* 2005; Kumar *et al.* 2007; Li *et al.* 2007; Kawakatsu *et al.* 2009; Rychert & Shearer 2009; Rychert *et al.* 2010; Fischer *et al.* 2010; Kind & Yuan 2010; Miller & Eaton 2010; Yuan & Romanowicz 2010). The depths of the lithospheric interfaces can be computed using the relative arrival times of converted waves observed on receiver functions and known or assumed distributions of seismic wave speeds between the discontinuities and the surface.

Surface waves at different periods sample different depth ranges in the crust and upper mantle. They offer tight constraints on the ver-

tical shear wave speed distributions in the lithosphere and asthenosphere and have long been used in lithospheric studies (e.g. Brune *et al.* 1963; Dziewonski & Anderson 1981; Levshin *et al.* 1989; Ekström 2000; Shapiro & Ritzwoller 2002; Maggi *et al.* 2006; Lebedev & van der Hilst 2008; Pasyanos 2010). Perhaps surprisingly, it has remained somewhat unclear to this day how sensitive surface waves are to the LAB depth and thickness and whether and how they can be used to constrain them. Van Heijst *et al.* (1994) considered a related question of surface wave sensitivity to the presence of a sublithospheric low-velocity zone (LVZ) and argued that the signal of LVZ properties in phase-velocity data did not exceed errors in the measurements, which they estimated at 1 per cent, random or systematic. Eaton *et al.* (2009) reviewed the multitude of definitions used to identify the LAB on shear-speed profiles computed by means of surface wave inversions. They argued, also, that the effect of LAB-thickness variations on surface wave phase velocities was negligible.

In this paper, we investigate specifically the sensitivity of surface wave phase velocities to the LAB depth and sharpness. We examine the sensitivity of both noise-free data and data with different levels of random noise. We then set up an elaborate grid-search inversion of phase-velocity curves for the LAB depth and thickness. Applications of the inversion procedure to synthetic and measured data demonstrate the resolving power of surface waves and indicate the levels of accuracy of surface wave measurements required for resolving the LAB depth and thickness.

2 SENSITIVITY

The depth sensitivity kernels of the fundamental-mode Rayleigh waves (the derivatives of the waves' phase velocity with respect to the shear speed at different depths) span the entire lithosphere–asthenosphere depth range (Fig. 1). The depth penetration and the shape of the kernels display a strong frequency dependence. Rayleigh-wave phase-velocity curves are certain to have some sensitivity to the properties of the LAB.

In this section, we explore how much phase velocities at different periods can change due to variations in the depth and thickness of the LAB. We also examine the impact of random noise in

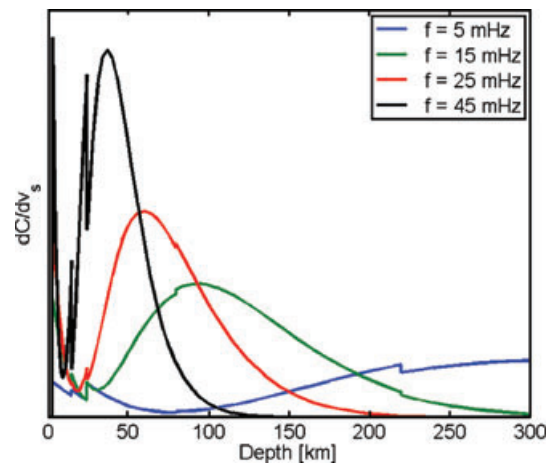


Figure 1. Fréchet derivatives of the phase velocity of the fundamental Rayleigh mode with respect to S -wave velocities at intermediate and long periods: 200 s period (5 mHz frequency), 67 s (15 mHz), 40 s (25 mHz) and 22 s (45 mHz). The derivatives are computed for the global-average Preliminary Reference Earth Model (PREM; Dziewonski & Anderson 1981).

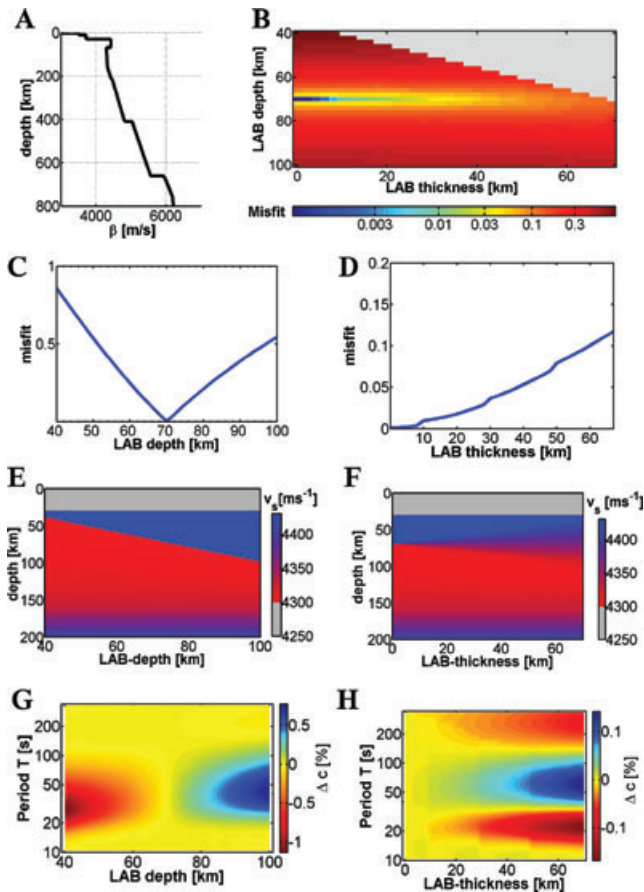


Figure 2. Sensitivity of Rayleigh-wave, phase-velocity data to the LAB depth and thickness. (a) An S -velocity profile; a phase-velocity curve is computed for this profile. (b) The S -velocity profile (a) is modified by varying the depth and thickness of the LAB. phase-velocity curves are calculated for the modified profiles and the misfit between the modified and original phase velocity curves is computed. The misfit is shown in the LAB depth-LAB thickness plane using the colour scale. (c) Misfit as a function of LAB depth, assuming the correct (zero) LAB thickness. (d) Misfit as a function of LAB thickness, assuming the correct (70 km) LAB depth. (e, f) the S -velocity models with varying LAB depths and thicknesses, respectively. (g, h) The period-dependent changes in synthetic phase-velocity curves due to variations in the LAB depth and thickness, respectively.

phase-velocity measurements on how detectable the LAB signal is in the data.

Fig. 2 illustrates the sensitivity of Rayleigh-wave phase velocities to the LAB depth and thickness. We first assume a shear-speed profile (Fig. 2a) with the LAB represented by a sharp, 0.1 km s^{-1} reduction in shear speed at a 70 km depth and compute a reference phase-velocity curve for this profile. We then modify the profile by varying the LAB depth in the 40–100 km range and LAB thickness in the 0–70 km range and compute dispersion curves for the profiles with the various combinations of LAB depths and thicknesses.

Variations in the LAB thickness are implemented by replacing the step change in shear speed at the LAB (Fig. 2a) with a linear gradient. The gradient is over a depth interval equal to the LAB thickness and is centred at the LAB-depth value.

Phase velocities are computed using a version of the MINOS modes code (Reference Earth Model web page <http://igppweb.ucsd.edu/~gabi/rem.dir/surface/minos.html>; Nolet 1990), streamlined for speed. The reference model is similar to AK135 (Kennett *et al.* 1995), apart from the lithosphere–asthenosphere depth range where

the structure is varied. Variations in S and P wave speeds are coupled [$\delta V_P (\text{m s}^{-1}) = \delta V_S (\text{m s}^{-1})$]. The quality-factor profile varies in concert with the shear-speed profile, with $Q = 400$ in the lithosphere and $Q = 75$ in the asthenosphere. (We verified that unless Q values are much lower than that, the effect of Q on the determination of LAB properties is small.)

Fig. 2(e) displays a family of shear-speed profiles with the LAB depth varying and the LAB thickness fixed at zero. Fig. 2(g) below shows how much phase velocities at different periods change due to the variations in the LAB depth. The phase-velocity variations are with respect to the reference curve computed for the reference profile in Fig. 2(a). Similarly, Fig. 2(f) shows profiles with a varying LAB thickness and the LAB depth fixed at 70 km, and Fig. 2(h) beneath it shows the corresponding phase-velocity variations.

Changes in the depth of the LAB result in changes in phase velocities in a range of periods (Fig. 2). For the LAB associated with a 0.1 km s^{-1} reduction in shear speed at a 70 km depth, a 10-km LAB-depth change produces changes in phase velocities of up to ~ 0.3 per cent. A 20 km decrease in the LAB depth produces a phase-velocity decrease of up to ~ 0.7 per cent; a 20 km increase in the LAB depth—a phase-velocity increase of up to ~ 0.5 per cent. The effect of the LAB thickness variations on phase velocities is much smaller. A phase-velocity change of 0.1 per cent requires an LAB-thickness change of over 40 km (assuming the 0.1 km s^{-1} shear-speed reduction across the LAB). The signal of the LAB-thickness change is enhanced, however, by the distinct frequency-dependent pattern of phase-velocity increases and decreases at frequencies just above and just below that of peak sensitivity to the LAB depth. Greater (or smaller) than 0.1 km s^{-1} shear-speed reductions at the LAB translate into greater (or smaller) effects of the LAB depth and thickness changes on the phase velocities.

Phase-velocity differences over the entire frequency range of the curve can be expressed by a single quantity, a misfit function, which we define as

$$F = \sum_i \frac{[C(f_i) - C_0(f_i)]^2}{[C_0(f_i)]^2}, \quad (1)$$

with the difference between the perturbed and reference phase velocities $C(f)$ and $C_0(f)$, respectively, sampled at densely spaced frequencies f_i . Frequency bands and sampling rates may vary from curve to curve, so that the absolute value of the misfit does not have any particular meaning, but the relative misfit variations due to perturbations of the same curve are meaningful. A logarithmic increase of the frequency spacing with frequency,

$$f_{i+1} - f_i \sim \log(f_i), \quad (2)$$

can help to equalize the weight of the structural information given by different parts of the phase-velocity curve, sensitive to different depth intervals in the Earth. With the logarithmic sample spacing, it will not matter whether phase velocities are sampled as a function of frequency or period.

Fig. 2(b) displays the misfit in the entire LAB depth-LAB thickness plane, and Figs 2(c) and (d) show misfit variations as a function of the LAB depth (with the LAB thickness fixed at 0) and as a function of the LAB thickness (with the LAB depth fixed at 70 km), respectively.

The frequency dependence of phase-velocity variations (Figs 2g and h) is clear and reflects the sensitivity of Rayleigh-wave phase velocities (Fig. 1). The global phase-velocity misfit function (Figs 2b–d) shows an unambiguous minimum at the true values of the LAB depth and thickness. The amplitude of the variations, however, is relatively small, especially for the LAB thickness

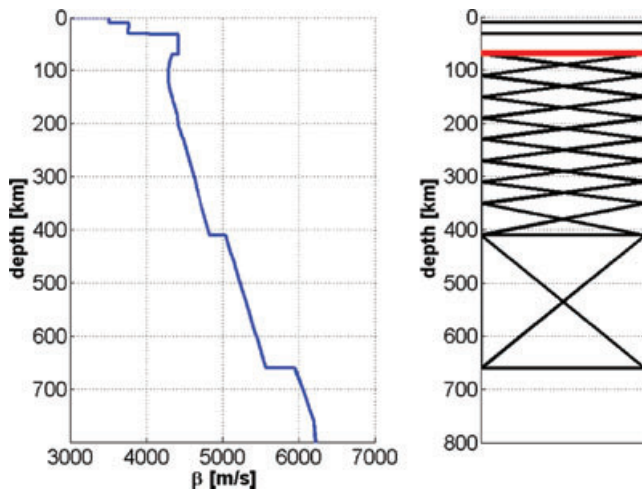


Figure 3. An example S -velocity profile (left-hand panel) and example parametrization (right-hand panel), as used in the tests and inversions. The crust and the thin mantle lithosphere in this example are parametrized with boxcar basis functions; the asthenosphere and deeper upper mantle—with triangular basis functions. The depth and width of the LAB are also varied in the tests and inversions.

changes. Will the LAB signal still be visible in the presence of noise in the data?

Assuming a reference shear-speed profile (Fig. 3, left-hand panel), we, again, compute phase velocities but now also add random noise to the phase-velocity curve, at levels from moderate (Fig. 4a) to strong (Figs 4e and i). The misfit (1) now quantifies the difference between phase-velocity curves $C(f)$ computed for shear-speed profiles with various LAB depths and thicknesses and the reference curve $C_0(f)$ with noise added. The tests in Fig. 4 show to what extent the LAB signal in phase-velocity data can be obscured by random noise.

We find that even strong random noise does not overwhelm the sensitivity of Rayleigh waves to the LAB depth. The misfit minimum is within a few kilometres of the correct value (70 km) in all of the tests (Fig. 4). This is because changes in the LAB depth produce a particular, smooth pattern of phase-velocity perturbation in a relatively broad frequency range. The thickness of the LAB, as constrained by surface wave data, should be expected to be less robust. In the presence of strong random noise (1.0 per cent) the misfit minimum is in the 20–30 km thickness range (Fig. 4i), substantially different from the correct value of 0 km.

In practice, phase-velocity measurements often display much less random noise than in Fig. 4(i). There may, however, be systematic measurement biases present as well (Section 6).

The tests in this section suggest that the sensitivity of Rayleigh-wave phase velocities to the depth of the LAB (expressed as a moderate reduction in shear speed) is sufficient for it to be resolved accurately. The sensitivity of the data to the LAB thickness is weaker, and the thickness cannot be expected to be resolved in all cases.

3 INVERSION

We now set up an inversion procedure for determination of LAB properties from surface wave phase velocities. This elaborate procedure is designed not only to locate best-fitting parameter ranges but also to establish the resolving power of surface waves in relation to the LAB depth and thickness and to display the structure of

the model space, in particular the subspace of the LAB depth and thickness.

The inversion is a grid search that comprises numerous non-linear gradient searches, one at each knot of the grid. We sample the LAB depth-LAB thickness plane uniformly and densely, using fine increments in both parameters. At each point on this plane, we perform a non-linear, gradient-search inversion. This inversion determines a best-fitting shear-speed profile. The profile minimizes the misfit as much as possible with the LAB depth and thickness fixed at the values that define this point on the plane. Any trade-offs between the LAB depth and thickness and shear speeds above and below the LAB will contribute to minimizing the impact of LAB properties on the misfit function (that is, the gradient-search inversion will compensate, as much as possible, the impact of changes in LAB properties with changes in shear speeds above and below the LAB). If the assumed LAB depth and thickness, however, are not consistent with the data, then the best possible fit will still be relatively poor.

Similar to (1), the misfit definition is

$$F = \sum_i \frac{[C_{\text{syn}}(f_i) - C(f_i)]^2}{[C(f_i)]^2}, \quad (3)$$

with the differences now being between synthetic and measured phase velocities $C_{\text{syn}}(f)$ and $C(f)$, respectively. The definition of the misfit and the set-up of the non-linear inversion are the same every time. The globally best-fitting ranges of LAB depths and thicknesses thus reveal the values most consistent with the data, with the trade-offs between the LAB properties and shear speeds above and below the LAB taken into account.

The non-linear gradient search is performed with the Levenberg-Marquardt algorithm, a modification of the Gauss algorithm and a special version of the Newton's method. Synthetic phase velocities are computed directly from a one-dimensional (1-D) Earth model at every step during the gradient search, using the MINOS modes code (<http://igppweb.ucsd.edu/~gabi/rem.dir/surface/minos.html>; Nolet 1990). The inversion is not linearized and converges to the true best-fitting solution (Erduran *et al.* 2008).

The LAB depth and thickness are fixed in each gradient-search inversion, but the wave speeds in both the crust and upper mantle are free to vary. This includes the seismic velocity change across the LAB, which is free to vary. The crust and mantle are parametrized with boxcar and triangle basis functions; a typical set of basis functions is shown in Fig. 3, right. If the mantle lithosphere layer is sufficiently thick, we parametrize its structure not with one boxcar basis function (Fig. 3) but with multiple triangular basis functions, as in inversions in Section 5. It is important that the crustal and mantle structure is overparametrized, i.e. that the number of basis functions is large enough so that the choice of a particular number does not affect the value of the minimum misfit achievable with various LAB depths and thicknesses. At the same time, the shear-speed profiles are constrained to be relatively smooth, both, implicitly, by the finite depth ranges of the basis functions (≥ 10 km in the crust; a few tens of km in the mantle) and by slight norm damping on the inversion parameters. With reasonably accurate phase-velocity measurements, small damping is sufficient to rule out exotic models with unrealistic shear-speed values. Any pre-existing knowledge regarding the crustal and mantle structure in the target location can be incorporated by either fixing or constraining *a priori* the relevant parameters (e.g. those for crustal structure or the Moho depth).

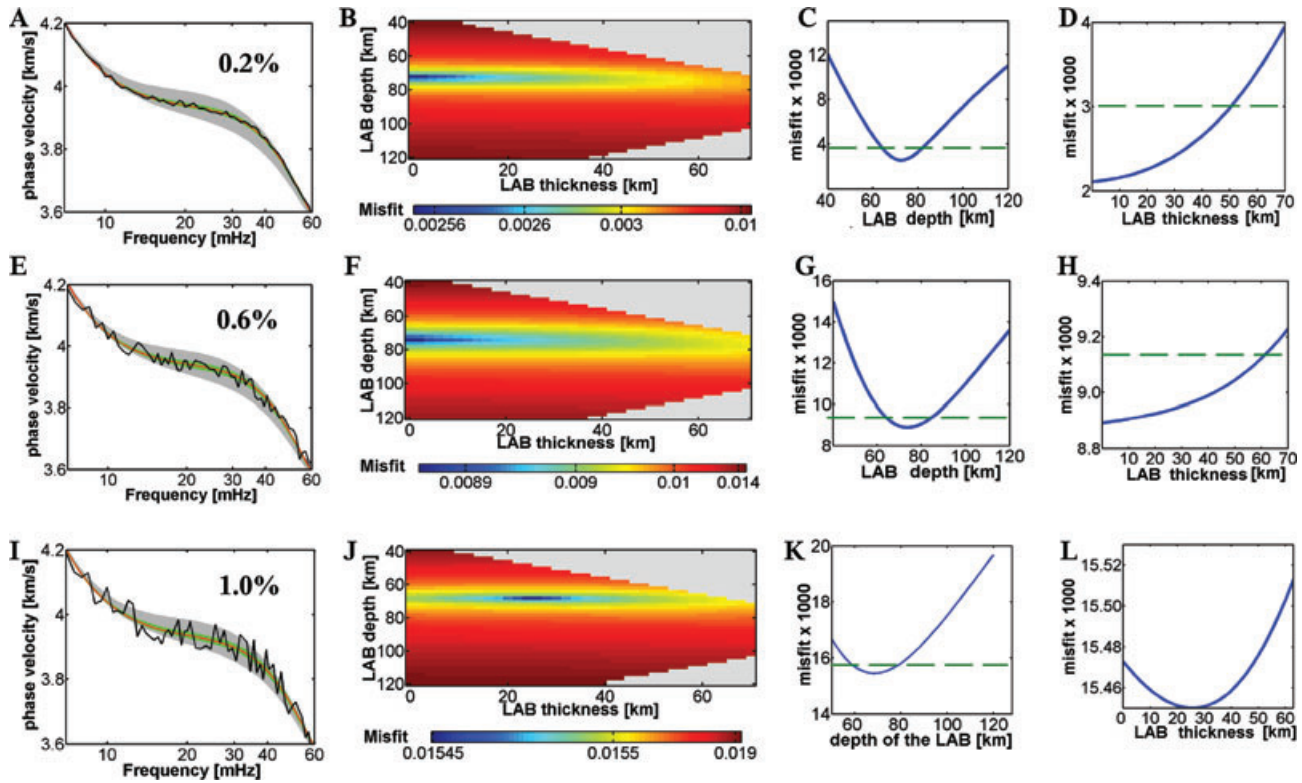


Figure 4. The effect of random noise in the data on the clarity of the signal of the LAB depth and thickness in Rayleigh-wave phase velocities. (a, e, i) Synthetic dispersion curves computed for the S -velocity profile in Fig. 3 (left-hand panel), with 0.2 per cent, 0.4 per cent, and 1.0 per cent random noise added, respectively. The grey bands around the curves contain all the synthetic dispersion curves computed for models with varying LAB depths and thicknesses (colour in b, f, j). The green bands contain the best-fitting curves. (b, f, j) Misfit between the original synthetic dispersion curves (a, e, i) and those computed for models with various LAB depths and thicknesses, for the different noise levels. (c, g, k) Misfit as a function of LAB depth, assuming the correct (zero) LAB thickness, for the different noise levels. (d, h, l) Misfit as a function of LAB thickness, assuming the correct (70 km) LAB depth, for the different noise levels. The dashed horizontal lines in (c, g, k, and d, h) show the misfit threshold for the best-fitting curves shown with green bands in (a, e, i). The dashed line in L falls outside the upper limit of the Y -axis (misfit axis).

4 RESOLUTION TESTS

We perform resolution tests in order to confirm that the inversion of phase-velocity curves can resolve the LAB accurately, as long as it is associated with a drop in shear speed. Fig. 5 illustrates three resolution tests. The three input 1-D models contain LAB as a sharp, 0.15 km s^{-1} reduction in shear speeds at the depths of 75, 60 and 75 km (Figs 5a, f and k, respectively). Synthetic phase-velocity curves computed from these input models have different amounts of noise added to them and are then inverted as data. Initial shear-speed profiles (dashed lines in Figs 5a, f and k) are used to define parametrizations and otherwise have no impact on the grid search.

It is useful to define thresholds for the misfit value so as to delimit the best-fitting ranges of the LAB depth and thickness. The dashed horizontal lines in the third and fourth columns from the left in Fig. 5 depict such thresholds, which we define—somewhat arbitrarily—so that the difference between the threshold value and the global misfit minimum equals 0.1 of the difference between the maximum misfit in the LAB depth-LAB thickness ranges sampled and the global misfit minimum. (This *ad hoc* definition can be updated, in future applications, using a more elaborate uncertainty-estimation approach (Section 6.2) but is sufficient for our purposes here).

Light-grey bands (Figs 5a, f and k) contain all profiles that minimize the misfit with the LAB depth and thickness fixed at various values within the ranges explored (Figs 5e, j and o). Narrower, green

bands contain best fitting models, with the misfit below the thresholds. These models are characterized by the most likely values of the LAB depth and thickness, according to the inversion. The (grey and green) bundles of synthetic dispersion curves (Figs 5b, g and l) correspond to the (grey and green) bundles of shear-speed profiles, respectively. The central (red) profile and dispersion curve indicate the globally best-fitting model.

Even in the presence of strong random noise, the inversion puts the LAB depth within a few kilometres of the correct value. The range of the best-fitting LAB depths, as defined by our choice of the misfit threshold, is 8–10 km, corresponding to an estimated measurement error of ± 5 km. The differences between the true and retrieved LAB depths are within these uncertainty ranges, suggesting that, in terms of the sensitivity of the data to the depth of an LAB (at a $\lesssim 100$ km depth), such measurement accuracy can be achieved.

The ranges of best-fitting LAB depths are broader in the inversions (Fig. 5) compared to those in sensitivity tests (Figs 2 and 4). This is because in the sensitivity tests the LAB depth and thickness values were the only differences between the shear-speed profiles corresponding to the different phase-velocity curves that were compared; otherwise, the profiles were fixed. In the inversions, the entire shear-speed profile is allowed to vary so as to minimize the misfit, given the particular LAB depth and thickness. The LAB properties trade-off with shear-speed values at depths near the LAB, and it is

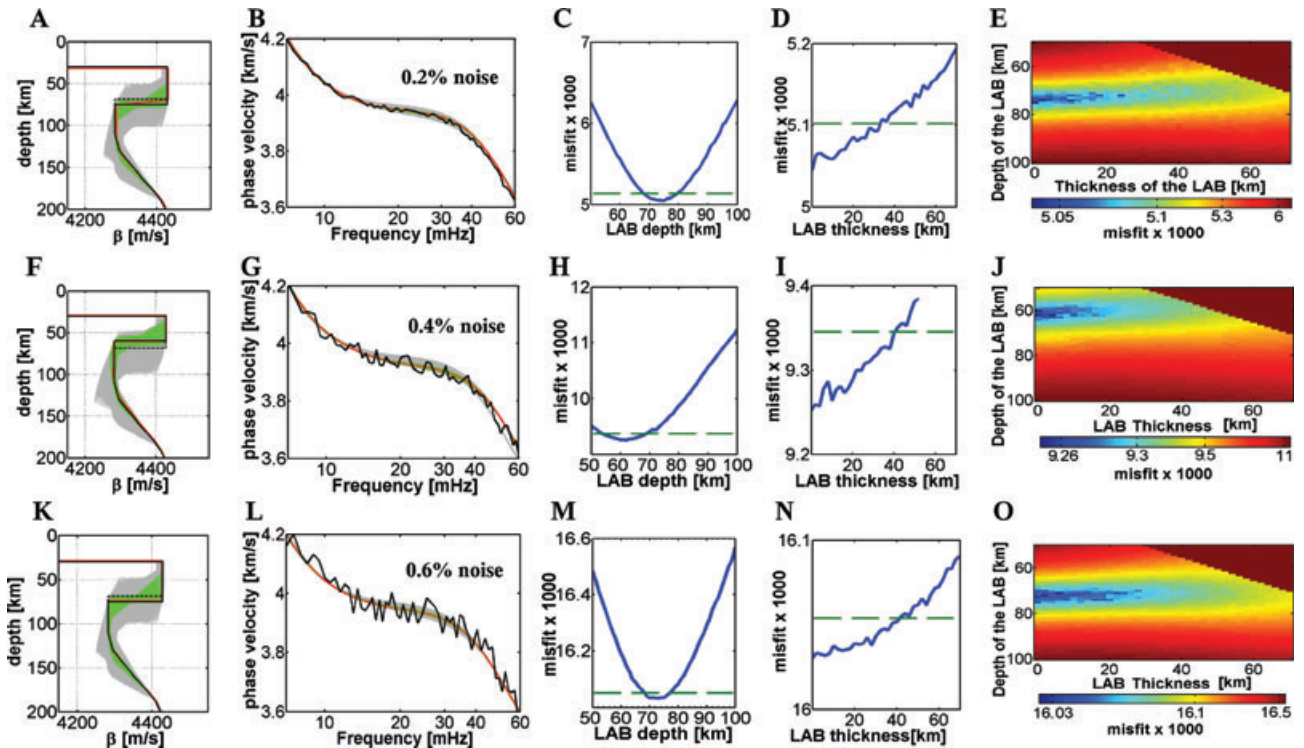


Figure 5. Resolution tests, with the inversion procedure exactly as applied to data in the following. Each row illustrates one test. (a, f, k) Solid black lines show the ‘real’ models (the shear-speed profiles for which synthetic phase-velocity curves were computed; these curves are considered data for the purposes of these tests). Dashed lines show the initial profiles used in the inversion. Grey bands contain all profiles that minimize the misfit with the LAB depth and thickness fixed at values within the ranges explored (e, j, o). Green bands show best fitting models (most likely values of the LAB depth and thicknesses). Red line shows the profile that produces the global misfit minimum. (b, g, l): Black: the ‘data’ dispersion curves. The phase velocities are computed for the models shown with solid black lines in a, f, k, with random noise added. The amplitude of the noise is specified within each frame. Grey and green bands contain the dispersion curves computed for shear-speed profiles within grey and green bands, respectively, in a, f, k. The red line shows the globally best-fitting dispersion curve. (c, h, m) Misfit as a function of the LAB depth, with the LAB thickness fixed at the correct value (0). The dashed green lines show the threshold that separates green and grey bundles of profiles (a, f, k). (d, i, n) Misfit as a function of the LAB thickness, with the LAB depth at correct values (as in the ‘input’ profiles in a, f, k). (e, j, o): Misfit (colour scale) as a function of the LAB depth and thickness. The value at each point within the depth-thickness plane is the result of a non-linear gradient search and is the best possible misfit given these values of the LAB depth and thickness.

due to these trade-offs that the ranges of best-fitting LAB-depth values broaden in the inversions (Fig. 5), compared to sensitivity tests (Figs 2 and 4). The misfit minima are still well defined, however, and are near correct LAB depths. This shows that the trade-offs do not obscure the relationship between the LAB depth and its signal in phase-velocity data, and we can use this signal in order to estimate the LAB depth. (We note that the inversion is restricted to reasonably smooth models, apart from the sharp shear-speed change at the LAB. This is achieved by the definition of relatively broad basis functions (Fig. 3, right-hand panel) and rules out exotic models with large, oscillatory shear-speed variations with depth that may also fit the phase-velocity data.)

Regarding the thickness of the LAB, both the families of best-fitting profiles (green in the column on the left, Fig. 5) and the distributions of the misfit (two columns on the right, Fig. 5) clearly show that it should be expected to be a less robust measurement, compared to the LAB depth. Even though the globally best-fitting LAB thickness values match the true thickness (0 km) closely, the LAB-thickness ranges defined by the misfit thresholds (Figs 5d, i and n) are broad and span values from 0 to 30–40 km. We conclude that although the measurement of the thickness of the LAB with surface wave dispersion data is possible in principle, the signal is relatively weak and the measurements will typically be less robust, compared to those of the LAB depth.

5 APPLICATION TO DATA: RESOLVING THE LAB BENEATH CONTINENTS

We now apply our technique to real data and investigate the LAB in two continental locations: western Germany and the Guyana Shield (Fig. 6). Western Germany is underlain by a Phanerozoic lithosphere with an asthenospheric low-velocity zone below (e.g. Bischoff *et al.* 2006; Lebedev & van der Hilst 2008). The Guyana Shield is an Archean craton with a cold, thick lithosphere; we choose this particular craton because it is underlain by a pronounced low-velocity zone (Lebedev *et al.* 2009), which should facilitate the LAB measurements.

We use broad-band, phase-velocity curves that have been measured previously for corridors between pairs of stations in the two locations (Fig. 7). The pairs of stations were: BFO (48.33°N, 8.33°E) – CLZ (51.84°N, 10.37°E) in Germany; PTGA (0.73°S, 59.97°W) – KOG (5.21°N, 52.73°W) and PTGA (0.73°S, 59.97°W) – MPG (5.11°N, 52.64°W) in the Guyana Shield. The measurements in western Germany were performed by Bischoff *et al.* (2006) with the elaborate cross-correlation method of Meier *et al.* (2004). The phase-velocity curves for the Guyana Shield (Lebedev *et al.* 2009) were measured with a combination of the cross-correlation (Meier *et al.* 2004) and multimode-waveform-inversion (Lebedev *et al.* 2005) approaches, so as to maximize the frequency range of the

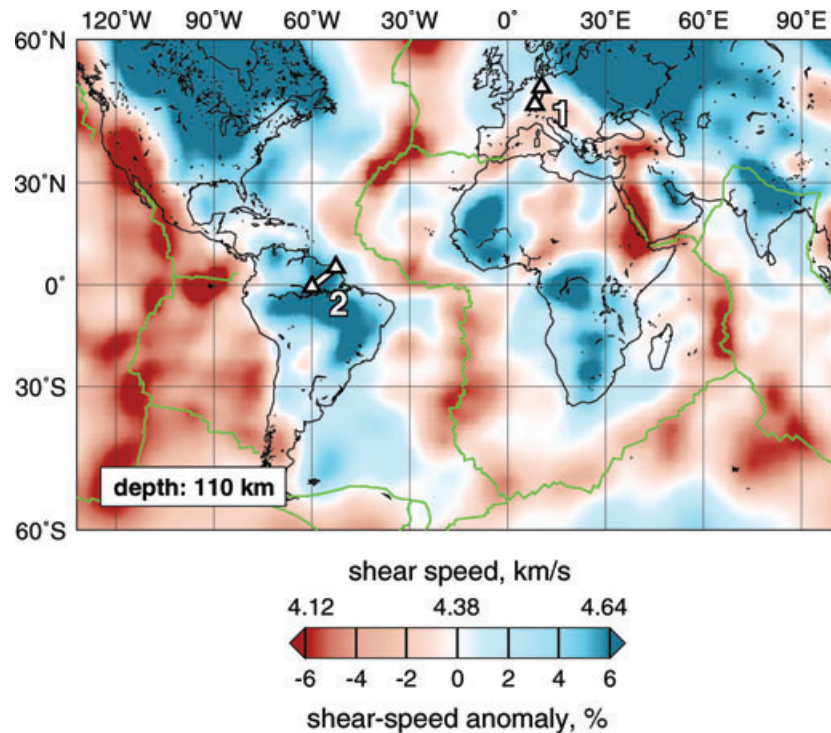


Figure 6. The two station pairs (triangles) and the interstation paths selected for LAB measurements. 1: Western Germany; 2: the Guyana Shield. The background shows shear wave speeds at a 110 km depth in the mantle according to the tomographic model of Lebedev & van der Hilst (2008). The reference period of the tomographic model is 50 s. Prominent high-velocity anomalies (dark blue) show stable Precambrian lithospheres, with the exception of high-velocity subducting plates in subduction zones. According to the large-scale tomography, western Germany (1) is characterized by relatively thin lithosphere and the Guyana Shield (2)—by thick lithosphere.

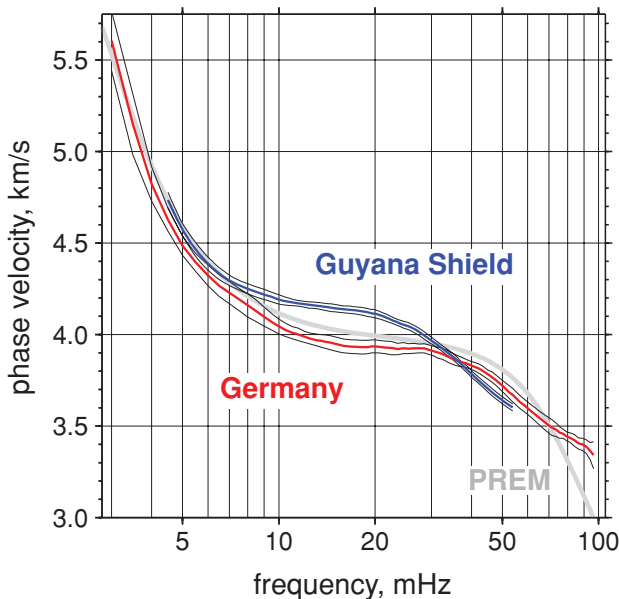


Figure 7. Rayleigh-wave, phase-velocity curves measured previously (Bischoff *et al.* 2006; Lebedev *et al.* 2009) for the two locations shown in Fig. 6. Each curve is averaged from measurements made using signal from tens of different earthquakes. Thin black lines show standard deviations.

measurements. The phase-velocity curves are averaged from 73 (Germany) and 42 (the Guyana Shield) one-event measurements and are accurate and robust.

The results of the inversion are summarized in Figs 8 and 9. The structure and thickness of the crust are taken from the earlier studies

(Bischoff *et al.* 2006; Tesauro *et al.* 2008; Lebedev *et al.* 2009). For the calculation of misfit functions, phase-velocity curve differences are sampled densely, with small frequency increments (86 and 175 samples along the Germany and Guyana curves, respectively).

The distribution of the misfit in the parameter space is similar to that in the tests. The LAB depth is constrained better than the LAB thickness. This suggests caution in interpretation of the best-fitting values of the LAB thickness.

The range of the best-fitting LAB depths beneath western Germany is 60–80 km, with the global misfit minimum around 70 km depth. In a recent joint inversion of Rayleigh-wave, phase-velocity data and magnetotelluric measurements from west-central Germany, Roux *et al.* (2011) found a range of 75–91 km and a best-fitting value of 84 km for the LAB depth. Geissler *et al.* (2010) used *S* receiver functions and inferred LAB depths between 80 and 100 km over western and central Germany. One difference between the inversion here and the inversion of Roux *et al.* (2011) is that here we neglected azimuthal anisotropy, whereas Roux *et al.* (2011) have accounted for azimuthal anisotropy by extracting their phase-velocity curves from anisotropic phase-velocity maps (Lebedev *et al.* 2007), which had isolated isotropic and anisotropic structure. (The anisotropic maps were constrained by the data set of Bischoff *et al.* (2006), of which the dispersion curve used here was a part.) In this study we apply our method directly to measured interstation curves, neglecting azimuthal anisotropy, and this may bias the result somewhat. Another reason for the difference may be that the structure of the lithosphere–asthenosphere system in western Germany is heterogeneous, and the nearby but different locations sampled in the different studies may not have exactly the same lithospheric thickness. In any case, the best-fitting LAB depth ranges overlap and are consistent.

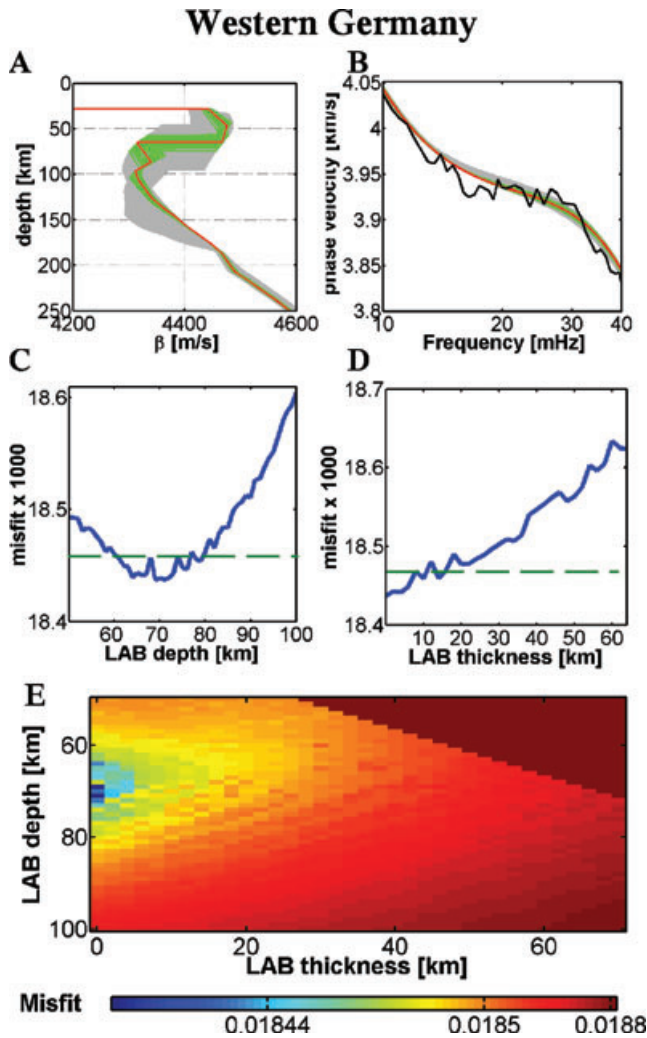


Figure 8. Inversion for the LAB depth and thickness beneath Western Germany. (a) the light-grey bundle contains all shear-speed profiles that minimize the misfit with the LAB depth and thickness fixed at values within the ranges explored (e). Green bands show best fitting models (most likely values of the LAB depth and thicknesses). The red line shows the profile that produces the global misfit minimum. (b) observed and synthetic dispersion curves, shown in the frequency range most sensitive to the LAB. Solid black line shows the measured dispersion curve. Grey and green bands contain the dispersion curves computed for shear-speed profiles within grey and green bands (a), respectively. The red line shows the globally best-fitting dispersion curve. (c) Misfit as a function of LAB depth, with the LAB thickness fixed at the best-fitting value (0). The dashed, horizontal green line shows the threshold that separates green and grey bundles (a, b). (d): Misfit as a function of LAB thickness, with the LAB depth fixed at the best-fitting value. (e) Misfit (colour scale) as a function of the LAB depth and thickness. The value at each point within the depth-thickness plane is the result of a non-linear gradient search and is the best misfit achievable given these values of the LAB depth and thickness.

Beneath the Guyana Shield, the best-fitting LAB depths are in the 140–175 km depth range, with the global misfit minimum at 160 km. This value for the middle of the shear-speed reduction depth range is consistent with typical shear-velocity profiles in cratonic lithospheres (e.g. Lebedev & Nolet 2003; Priestley & McKenzie 2006; Lebedev *et al.* 2009; Eaton *et al.* 2009; Fishwick 2010), and can be reconciled with models and arguments regarding the chemical and thermal boundary layers beneath cratons (e.g. Griffin *et al.* 2003; Lee *et al.* 2005; O'Reilly & Griffin 2010).

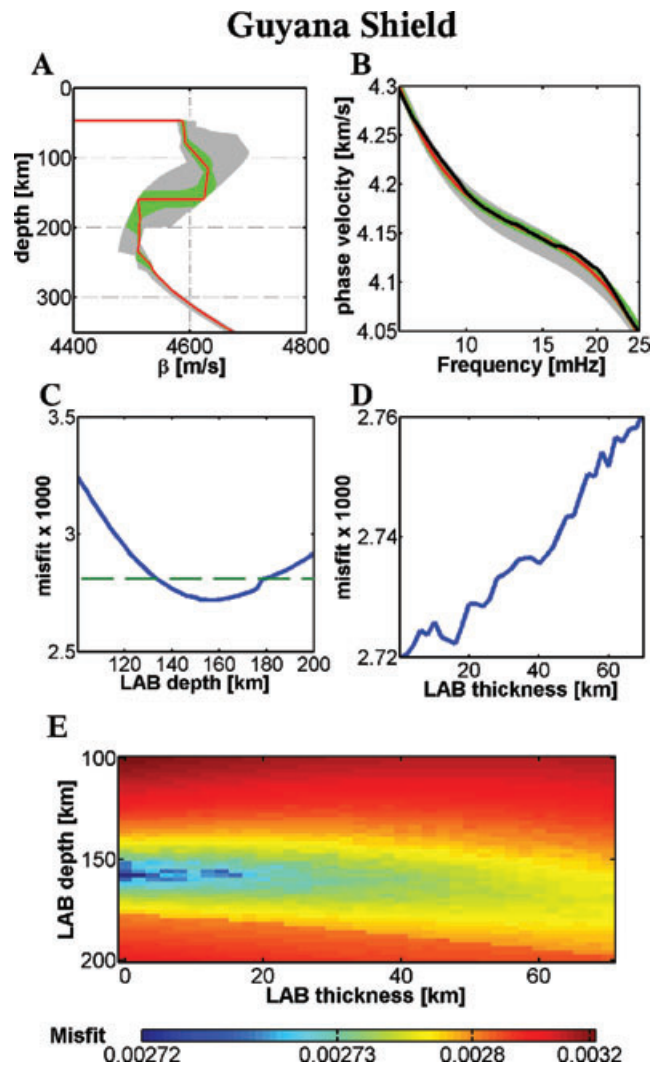


Figure 9. Inversion for the LAB depth and thickness beneath the Guyana Shield. The content of the different frames is as in Fig. 8. The dashed line (misfit threshold) is not plotted in D because the threshold exceeds the upper limit of the Y (misfit) axis.

To summarize, the applications of our phase-velocity analysis to measured data confirm its potential to resolve LAB properties in different tectonic settings. The LAB depth-LAB thickness parameter subspace shows a simple structure with unambiguous regions of best-fitting values, just like in the tests with synthetic data. The smallest-misfit regions define the ranges of the most likely LAB depths. For the LAB thickness, the ranges are, typically, wider. The LAB depths that we determine beneath the two continental locations are broadly consistent both with what can be expected from the regions' tectonic settings and with the results of published work on shear-speed profiles or LAB depth in the regions (Bischoff *et al.* 2006; Lebedev *et al.* 2009; Roux *et al.* 2011, and references therein).

6 DISCUSSION

6.1 Sensitivity of surface waves to the LAB

We have investigated resolving an LAB expressed as a reduction in shear speeds, from the high-velocity lithosphere to the low-velocity

asthenosphere. Such reduction may be common but not necessarily ubiquitous in the Earth. The LAB is a dynamic boundary and both the lithosphere and asthenosphere are heterogeneous, in particular beneath continents. The lithosphere–asthenosphere contrast in seismic velocities is not the same everywhere—nor is it even evident everywhere (e.g. Lebedev *et al.* 2009).

Phase-velocity curves are sensitive to an LAB as a drop in shear velocities from the lithosphere to the asthenosphere. The drop may be sharp (over a depth interval of a few kilometres) or gradual (a few tens of kilometres). In either case, the LAB depth that we resolve with phase-velocity curves is the depth of the middle of this interval. If the decrease in shear speed at the base of the lithosphere is over a depth interval but is not linear within it, then the surface wave resolved LAB depth will deviate from the middle of the interval towards where the decrease is steeper.

The relationships between the depth range of the shear-speed reduction at the LAB and the thermal, compositional and mechanical definitions of the lithosphere have been discussed elsewhere (e.g. Griffin *et al.* 2003; Lee *et al.* 2005; Artemieva 2009; Eaton *et al.* 2009; Kawakatsu *et al.* 2009; Fischer *et al.* 2010). With the nature of the LAB debated, more observational evidence is needed to advance our understanding of this boundary, and our focus here is on extracting such evidence from surface wave data. In relation to the different LAB definitions, we note that the LAB depth most naturally constrained by surface wave data is the depth of the middle of the depth range in which shear speed decreases with depth. If this range is broad, then the surface wave derived LAB depth will be shallower (by half-width of the range) than the depth of the bottom of the thermal lithosphere, if that is understood as the boundary between the domains of conductive and convective heat transfer and estimated to coincide with the bottom of the shear-speed-reduction depth range. Joint analysis of surface waves and receiver functions, the latter sensitive to sharp discontinuities within the Earth, has proved effective in studies of discontinuities from the crust down to deep upper mantle (e.g. Julià *et al.* 2000; Lebedev *et al.* 2002; Lebedev *et al.* 2003; Endrun *et al.* 2004; Endrun *et al.* 2005; Endrun *et al.* 2008) and can enhance the resolution of the fine structure of the LAB, as well as of any discontinuities within the lithosphere that may be present.

The sensitivity of phase-velocity curves to the LAB depth and thickness is evident and easily quantified (Section 2). The signal of LAB properties in phase-velocity data is relatively small, typically a few tenths of 1 per cent. It is, however, a smooth perturbation over a broad frequency range, and our tests suggest that this signal is sufficient for robust estimation of the LAB depth, provided that phase-velocity data do not contain substantial systematic biases. Model-parameter trade-offs, inversion non-uniqueness, and random noise in the data all result in LAB-depth-estimate uncertainty of only a few kilometres. Sensitivity of phase velocities to the LAB thickness is weaker, and surface wave LAB-thickness measurements, although possible in principle, will require higher phase-velocity curve accuracy, compared to LAB-depth measurements.

6.2 Uniqueness of inversion solutions

In inversions of phase-velocity data, the LAB depth and thickness trade-off with the shear-speed structure above and below the LAB. Both these trade-offs and errors in the data contribute to non-uniqueness of the models that are the results of the inversions. The effect of the trade-offs can be seen, for example, in the broadening of the best-fitting LAB-depth ranges—from those in our sensitivity

tests (Figs 2 and 4: no inversions, no trade-offs) to those in the inversions of synthetic and real data (Figs 5, 8 and 9: inversions, trade-offs making an impact). Broader smallest-misfit valleys in the LAB depth-LAB thickness plane indicate larger uncertainties of the LAB-depth measurements. The broadening of the valleys, however, is limited, and their shape and position are stable, which confirms the robustness of the inversion results.

The *ad hoc* definitions of misfit thresholds that we used to estimate LAB measurement uncertainties (Figs 4, 5, 8 and 9) can be replaced, in future applications, with more quantitative uncertainty estimates. For example, we could fit a parabola $e(p)$ to the misfit curve (the misfit as a function of a parameter p) in the vicinity of the p_{\min} that minimizes the misfit:

$$e(p) = e_0 + c(p - p_{\min})^2. \quad (4)$$

The curvature c will then give an explicit estimate for the resolution of the parameter p (e.g. the LAB depth).

One parameter we did not vary in the inversions (Figs 8 and 9) is the Moho depth. If the mantle lithosphere is relatively thin, and especially if the crust is thick, incorrect Moho depths can bias any estimates of the LAB properties. Regarding our inversions in Section 5, the Moho depth beneath west-central Germany is well known from published work (Tesauro *et al.* 2008, and references therein), and for the thick lithosphere of the Guyana Shield the trade-off will be small. We note, however, that either incorporation of existing constraints on the Moho depth or its inclusion as an inversion parameter are essential for the LAB mapping accuracy.

The simple structure of the LAB depth-LAB thickness parameter subspace, with one clearly defined smallest-misfit valley, is robust, similar in tests and data inversions, and unaffected by random errors in the data. The shape of the valley shows that the LAB depth and LAB thickness parameters have uncorrelated uncertainties (do not trade off with each other), with the LAB thickness more uncertain compared to the LAB depth.

6.3 Effects of random errors in phase-velocity curves

We consider errors in phase-velocity measurements to be random if they are uncorrelated and vary randomly and independently at points a few mHz away from each other along the frequency axis (e.g. Figs 4 and 5). The clarity of the signal of the LAB depth in phase-velocity data is not affected by such random errors (Fig. 4). The signal of the LAB thickness, in contrast, can be obscured by strong random noise (1.0 per cent), which will result in errors in LAB-thickness estimates (Fig. 4).

Resolution tests (Fig. 5) show that even when phase-velocity curves are contaminated by strong random noise, an inversion of the curves resolves the LAB depth accurately, with an error of only a few kilometres. The LAB thickness is less likely to be resolved if large random errors are present.

The measured phase-velocity curve that we selected from the Germany data set of Bischoff *et al.* (2006) displays a higher noise level compared to the other curve we use (Figs 7–9) and is, also, noisier than some of the other curves in that data set, measured using seismograms from the German Regional Seismic Network (GRSN; Bischoff *et al.* 2006). Because our purpose is to test the inversion for LAB properties on a range of different synthetic and real data, we used this curve with clearly visible noise. The effect of the noise is similar to that seen in resolution tests (Fig. 5), and the inversion results do not appear biased by the random noise (although they may be affected by a systematic bias in phase velocities due

to azimuthal anisotropy, which we neglected). Random noise in the other real-data example is smaller (Figs 7 and 9).

How large are the errors of phase-velocity measurements made with today's data and today's methods? These errors are not straightforward to estimate. The phase-velocity curves in Fig. 7 are plotted with their standard deviations. The standard errors of the mean are much smaller, comparable to the line thickness in Fig. 7, regardless of whether they are computed from the measurements and their quantity directly or by the 'bootstrap' method (Efron & Tibshirani 1991). We note, however, that if standard deviations are large—for example, substantially larger than in Fig. 7—this will indicate an increased probability of systematic biases in the average curve due to diffraction or mode interference; measurements with large standard deviations are unlikely to be suitable for resolving the LAB.

Of course, interstation measurements are only one method of measuring surface wave dispersion. More sophisticated surface wave analysis techniques should yield more and more accurate phase-velocity measurements, which can then be used to resolve the LAB.

6.4 Effects of systematic biases in phase-velocity curves

We define systematic biases here as errors that persist (change little) across relatively broad period ranges (tens of seconds, at periods sampling the LAB). If a phase-velocity curve is measured with a two-station approach, for example, and azimuthal anisotropy is present—say, in the asthenosphere—then the measured dispersion curve will be azimuth-specific. If this curve is inverted for LAB properties as an isotropic-average curve, this may give rise to a bias, depending on the orientation of the anisotropic fabric and station locations. If the fast-propagation azimuth is parallel to the station-station azimuth, for instance, then the asthenosphere will appear to be too fast, and if the two azimuths are perpendicular it will appear to be too slow. In either case, LAB property estimates may be affected.

Systematic biases in two-station phase-velocity measurements can also be caused by diffraction and mode interference (Friederich *et al.* 2000; Pedersen 2006; Tanimoto & Prindle 2007; Bodin & Maupin V. 2008). Averaging many measurements performed on signal from events in different regions, particularly at opposite azimuths from the station-station pair, reduces these biases (Meier *et al.* 2004; Lebedev *et al.* 2006), but it is difficult to estimate the amplitude of systematic errors that remain. A large standard deviation of a set of same-station-pair measurements is one warning sign of a high probability of systematic errors. Numerical benchmarking studies with realistic assumed Earth structure and distributions of sources and stations is an increasingly effective means of evaluating the biases (e.g. Bodin & Maupin 2008; Qin *et al.* 2008).

In our inversions of measured dispersion curves, we found LAB depths broadly consistent with reasonable expectations for the regions and with published models. This is encouraging and suggests that LAB measurements should be possible with some of the high-quality, broad-band, phase-velocity data available at present. Comparing the measured and synthetic phase-velocity curves (Figs 8 and 9), we find some small but persistent discrepancies over a relatively broad frequency range of 17–22 mHz (45–59 s) for the Guyana inversion. (In the curve from Germany, moderate systematic biases also appear to be present but random errors dominate.) Such discrepancies, in particular where the measured curve is not as smooth as a fundamental-mode phase-velocity curve must be, given the broad fundamental-mode depth sensitivity kernels (Fig. 1), indi-

cate errors in the data in these frequency ranges. Such errors cause broadening of the smallest-misfit valleys in the LAB depth-LAB thickness planes and contribute to measurement uncertainties.

The continuing improvement in methods and the rapid growth of broadband seismic networks translate into higher and higher accuracy of phase-velocity measurements. Some of the surface wave data available today is already accurate enough for resolving the LAB; more of such data is likely to become available in the near future.

6.5 Using surface waves for LAB mapping

With the sensitivity of surface waves to LAB properties evident, what surface wave analysis methods will be most effective for LAB mapping? Because the signal of the LAB properties in surface wave data is relatively small, the accuracy of surface wave measurements is critical and will determine which approaches—existing or under development—turn out to be the most effective.

We have, so far, considered phase velocities of Rayleigh waves only. Love waves—the surface waves associated with horizontally polarized shear waves—also sample the entire lithosphere–asthenosphere depth range and can provide additional information regarding the LAB. Van Heijst *et al.* (1994) investigated the expression of an asthenospheric low-velocity zone in Love and Rayleigh wave data and found the signal in phase velocities of both types of waves to be similar in amplitude. In this paper we have focussed on resolving the LAB with Rayleigh waves, because Rayleigh-wave measurements are more abundant and, often, have smaller errors. We note, however, that an addition of Love wave data, where available, will increase the resolving power of surface waves in relation to the LAB, both because complementary constraints on LAB properties will be added and because radial anisotropy of the lithosphere and asthenosphere will be constrained (e.g. Van Heijst *et al.* 1994; Gung *et al.* 2003; Nettles & Dziewonski 2008; Yoshizawa *et al.* 2010). Radial anisotropy is caused by fabric within the lithosphere; once it is known, we can determine isotropic-average shear speeds that reflect temperature and composition at depth.

Interstation phase-velocity curves can be measured with a two-station approach, with either cross-correlations or waveform inversions or both (e.g. Meier *et al.* 2004; Lebedev *et al.* 2006), and inverted for LAB properties, as we have done in Section 5. The advantage of this approach is that phase-velocity measurements are inverted for LAB directly, with no intermediate inversion steps. A disadvantage is that if substantial azimuthal anisotropy is present in the lithosphere or asthenosphere, it will not be accounted for and can bias the inferences regarding the LAB.

Cross-correlation measurements of the fundamental-mode phase velocities can be done if the fundamental mode can be isolated from the higher modes. For most seismograms, this can be achieved in broad period ranges by means of time-frequency filtering and windowing (Meier *et al.* 2004). Multimode waveform inversions (e.g. Cara & Lévêque 1987; Nolet 1990; Debayle & Kennett 2000; Yoshizawa & Kennett 2002; Lebedev *et al.* 2005) make use of mode summation to model complete waveforms and can provide phase-velocity measurements regardless of mode interference. In addition to phase velocities of the fundamental mode, those of the higher modes can also be measured (e.g. Lebedev *et al.* 2005; Visser *et al.* 2007) and used as additional constraints on mantle structure (Visser *et al.* 2008; Yoshizawa & Ekström 2010), including the LAB properties (Van Heijst *et al.* 1994).

A straightforward way to target the LAB with either phase-velocity measurements or waveform inversions would be to invert phase-velocity data or waveforms for the average LAB depths between earthquakes and stations. The main practical difficulty with such ‘source-station’ inversions will be due to uncertainties in the earthquake locations and origin times and in earthquake source mechanisms (e.g. Muzyert & Snieder 1996; Levshin *et al.* 1999; Lebedev *et al.* 2005), which can affect LAB estimates significantly.

Tomographic inversions of large sets of source-station measurements for phase-velocity maps will average out random, earthquake-source errors to a large extent. In areas sampled by broadband seismic-station arrays, array analysis can remove the effects of source uncertainties (almost) entirely. Regional phase-velocity maps or region-average, phase-velocity curves can be computed either by tomographic inversions of multiple interstation measurements or by other methods (e.g. Pedersen 2006; Yang & Forsyth 2006; Tanimoto & Prindle 2007; Zhang *et al.* 2007; Zhang *et al.* 2009; Lin *et al.* 2009). If robust phase-velocity maps are determined in sufficiently broad period ranges—including the range where the sensitivity to the LAB peaks and the adjacent ranges at shorter and longer periods—then phase-velocity curves can be constructed and inverted for LAB properties point by point.

Phase-velocity maps will have a particular advantage as a source of phase-velocity curves if they are computed with both isotropic and azimuthally anisotropic heterogeneity included. (Region-average phase-velocity curves can also be computed, using array data, so as to account for azimuthal anisotropy, e.g. Pedersen 2006; Yang & Forsyth 2006). If anisotropic signal can be accounted for and isolated, inversions of isotropic-average, phase-velocity curves for LAB properties will not be biased by anisotropy. We also note that anisotropy itself can be used to locate the LAB if the boundary is associated with a change in anisotropic fabric orientation (e.g. Debayle & Kennett 2000; Plomerová *et al.* 2002; Simons *et al.* 2002; Debayle *et al.* 2005; Deschamps *et al.* 2008b; Yuan & Romanowicz 2010), although in this paper we have focussed on the isotropic-average seismic wave speeds.

The emergence of large, dense arrays of broadband seismic stations should make possible significant further improvements in the accuracy of surface wave measurements. Inversions of array data for both phase-velocity distributions and the evolution of wavefields promise to minimize biases in the measurements due to surface wave diffraction (Friederich & Wielandt 1995). The increasing feasibility of using (quasi-)exact numerical solutions for the forward wave-propagation problem also holds a promise to increase the accuracy of structural information extracted from seismograms (e.g. Komatitsch *et al.* 2002). On-going improvements in surface wave measurements can be translated into tighter constraints on LAB properties by means of inversions such as the one set up in this paper.

7 CONCLUSIONS

Surface waves show clear, unambiguous sensitivity to the location of a shear-speed reduction from the lithosphere to the asthenosphere. Wherever the lithosphere–asthenosphere boundary is associated with such a shear-speed reduction, surface waves can be used to locate it. Because variations in LAB properties translate into relatively small variations in phase velocities, highly accurate surface wave measurements are required for resolving the LAB with useful precision.

Sensitivity tests with an LAB associated with a 2–3 per cent shear speed reduction at <100 km depth show that 10–20 km variations in the LAB depth translate into phase-velocity changes of up to 1 per cent. Variations in the thickness of the LAB from 0 to a few tens of kilometres translate into phase-velocity changes of only 0.1 per cent, although the signal of the LAB-thickness variations is enhanced by a distinct pattern of phase-velocity increases and decreases at frequencies above and below that of peak sensitivity to the LAB depth.

We have set up an inversion of phase-velocity curves for the LAB depth and thickness, comprising dense grid sampling of the LAB depth-LAB thickness parameter plane and non-linear, gradient-search inversions at every point. This inversion procedure accounts for the model non-uniqueness due to trade-offs of the LAB properties with shear-speed structure above and below the LAB. Application of the inversion to synthetic and measured data confirms the feasibility of LAB mapping with surface waves and displays the properties of the LAB depth-LAB thickness parameter subspace.

Grid-search inversions of phase-velocity curves for the LAB depth and thickness (defined as the middle of a depth interval with a linear shear-speed decrease in it and the width of this interval, respectively), show that the two parameters have uncorrelated uncertainties, with the LAB depth constrained better than the LAB thickness. The structure of the LAB depth-LAB thickness parameter plane is simple and robust, with a single, clearly defined smallest-misfit valley.

The middle of the shear-speed-reduction depth range is the natural definition of the LAB for the purposes of surface wave inversions, dictated by the sensitivity of the data. If the decrease in shear speed within the range is not linear, then surface wave inversions will place the LAB depth closer to where it is steeper. Fine layering within the LAB depth range cannot be resolved with surface waves alone; joint analysis of surface waves and receiver functions—or other data sensitive to the sharpness of radial shear-speed gradients—can enhance the resolution of the location and fine structure of the LAB.

Random errors in phase-velocity measurements have a limited effect on LAB-depth measurements, causing errors of only a few kilometres. Measurements of the LAB thickness are less robust and will not be possible in the presence of large (~1 per cent) random errors. Substantial systematic biases in the measurements can affect both LAB-depth and LAB-thickness estimates; phase-velocity curves with such biases are not suitable for inversions for LAB properties.

Resolving the LAB requires very accurate surface wave measurements. In our view, this is already possible with some of the phase-velocity data available today. On-going expansion of dense seismic networks, accompanied by developments in seismic analysis methods, should make it increasingly feasible to map the LAB with surface waves around the globe.

ACKNOWLEDGMENTS

Detailed, insightful reviews by K. Yoshizawa and S. Fishwick have helped us to improve the manuscript. Figs 6 and 7 were generated with Generic Mapping Tools (Wessel & Smith 1995). This work was supported by Science Foundation Ireland (grant 08/RFP/GEO1704 awarded to S. Lebedev).

REFERENCES

- Anderson, D.L. & Sammis, C., 1970. Partial melting in the upper mantle, *Phys. Earth planet. Inter.*, **3**, 41–50.

- Artemieva, I.M., 2009. The continental lithosphere: reconciling thermal, seismic, and petrologic data, *Lithos*, **109**, 23–46.
- Bischoff, M., Endrun, B. & Meier, T., 2006. Lower crustal anisotropy in Central Europe deduced from dispersion analysis of Love and Rayleigh waves, *Geophys. Res. Ab.*, **8**, 10010, European Geosciences Union.
- Bodin, T. & Maupin, V., 2008. Resolution potential of surface wave phase velocity measurements at small arrays, *Geophys. J. Int.*, **172**, 698–706.
- Brune, J. & Dorman, J., 1963. Seismic waves and earth structure in the Canadian Shield, *Bull. seism. Soc. Am.*, **53**, 167–210.
- Cara, M. & Lévêque, J.J., 1987. Waveform inversion using secondary observables, *Geophys. Res. Lett.*, **14**, 1046–1049.
- Dalton, C.A., Ekström, G. & Dziewonski, A.M., 2008. The global attenuation structure of the upper mantle, *J. geophys. Res.*, **113**, B09303, doi:10.1029/2007JB005429.
- Darbyshire, F.A. & Lebedev, S., 2009. Rayleigh wave phase–velocity heterogeneity and multi-layered azimuthal anisotropy of the Superior Craton, Ontario, *Geophys. J. Int.*, **176**, 215–234.
- Debayle, E. & Kennett, B.L.N., 2000. The Australian continental upper mantle; structure and deformation inferred from surface waves, *J. geophys. Res.*, **105**, 25 423–25 450.
- Debayle, E., Kennett, B.L.N. & Priestley, K., 2005. Global azimuthal seismic anisotropy and the unique plate-motion deformation of Australia, *Nature*, **433**, 509–512.
- Deschamps, F., Lebedev, S., Meier, T. & Trampert, J., 2008a. Azimuthal anisotropy of Rayleigh-wave phase velocities in the east-central United States, *Geophys. J. Int.*, **173**, 827–843.
- Deschamps, F., Lebedev, S., Meier, T. & Trampert, J., 2008b. Stratified seismic anisotropy reveals past and present deformation beneath the East-central United States, *Earth planet. Sci. Lett.*, **274**, 489–498.
- Dziewonski, A.M. & Anderson, D.L., 1981. Preliminary reference Earth model, *Phys. Earth planet. Inter.*, **25**, 297–356.
- Eaton, D.W., Darbyshire, F., Evans, R.L., Grütter, H., Jones, A.G. & Yuan, X., 2009. The elusive lithosphere–asthenosphere boundary (LAB) beneath cratons, *Lithos*, **109**, 1–22.
- Efron, B. & Tibshirani, R., 1991. Statistical Data Analysis in the Computer Age, *Science*, **253**, 390–395.
- Ekström, G., 2000. Mapping the lithosphere and asthenosphere with surface waves: lateral structure and anisotropy, in *The History and Dynamics of Global Plate Motions*, pp. 277–288, eds Richards, M.A., Gordon, R.G., van der Hilst, R.D., Geophys. Monograph No. 121. AGU.
- Endrun, B., Meier, T., Bischoff, M. & Harjes, H.-P., 2004. Lithospheric structure in the area of Crete constrained by receiver functions and dispersion analysis of Rayleigh phase velocities, *Geophys. J. Int.*, **158**, 592–608.
- Endrun, B., Ceranna, L., Meier, T., Bohnhoff, M. & Harjes, H.-P., 2005. Modeling the influence of Moho topography on receiver functions: a case study from the central Hellenic subduction zone, *Geophys. Res. Lett.*, **32**, L12311, doi:10.1029/2005GL030666.
- Endrun, B., Meier, T., Lebedev, S., Bohnhoff, M., Stavrakakis, G. & Harjes, H.-P., 2008. S velocity structure and radial anisotropy in the Aegean region from surface wave dispersion, *Geophys. J. Int.*, **174**, 593–616.
- Endrun, B., Lebedev, S., Meier, T., Tirel, C. & Friederich, W., 2011. Complex layered deformation within the Aegean crust and mantle revealed by seismic anisotropy, *Nat. Geosci.*, **4**, 203–207, doi: 10.1038/NCEO1065.
- Erduran, M., Endrun, B. & Meier, T., 2008. Continental vs. oceanic lithosphere beneath the eastern Mediterranean Sea—implications from Rayleigh wave dispersion measurements, *Tectonophysics*, **457**, 42–52.
- Evans, R.L., Hirth, G., Baba, K., Forsyth, D., Chave, A. & Mackie, R., 2005. Geophysical evidence from the MELT area for compositional controls on oceanic plates, *Nature*, **437**, 249–52.
- Farra, V. & Vinnik, L., 2000. Upper mantle stratification by P and S receiver functions, *Geophys. J. Int.*, **141**, 699–712.
- Fischer, K.M., Ford, H.A., Abt, D.L. & Rychert, C.A., 2010. The lithosphere–asthenosphere boundary, *Ann. Rev. Earth planet. Sci.*, **38**, 551–575.
- Fishwick, S., Kennett, B.L.N. & Reading, A.M., 2005. Contrasts in lithospheric structure within the Australian craton—insights from surface wave tomography, *Earth planet. Sci. Lett.*, **231**, 163–176.
- Fishwick, S., 2010. Surface wave tomography: imaging of the lithosphere–asthenosphere boundary beneath central and southern Africa? *Lithos*, **120**, 63–73.
- Frederiksen, A.W., Miong, S.-K., Darbyshire, F.A., Eaton, D.W., Rondenay, S. & Sol, S., 2007. Lithospheric variations across the Superior Province, Ontario, Canada: evidence from tomography and shear wave splitting, *J. geophys. Res.*, **112**, B07318, doi:10.1029/2006JB004861.
- Friederich, W., Hunzinger, S. & Wielandt, E., 2000. A note on the interpretation of seismic surface waves over three-dimensional structures, *Geophys. J. Int.*, **143**, 335–339.
- Friederich, W. & Wielandt, E., 1995. Interpretation of seismic surface-waves in regional networks—joint estimation of wave-field geometry and local phase–velocity—method and numerical tests, *Geophys. J. Int.*, **120**, 731–744.
- Fulla, J., Fernández, M., Afonso, J.C., Vergés, J., Zeyen, H., 2010. The structure and evolution of the lithosphere–asthenosphere boundary beneath the Atlantic-Mediterranean Transition Region, *Lithos*, **120**, 74–95.
- Gaherty, J.B. & Jordan, T.H., 1995. Lehmann Discontinuity as the base of an anisotropic layer beneath continents, *Science*, **268**, 1468–1471.
- Gaherty, J.B., Kato, M. & Jordan, T.H., 1999. Seismological structure of the upper mantle: a regional comparison of seismic layering, *Phys. Earth planet. Inter.*, **110**, 21–41.
- Geissler, W.H., Sodoudi, F. & Kind, R., 2010. Thickness of the central and eastern European lithosphere as seen by S receiver functions, *Geophys. J. Int.*, **181**, 604–634.
- Griffin, W.L., O'Reilly, S.Y., Abe, N., Aulbach, S., Davies, R.M., Pearson, N.J., Doyle, B.J. & Kivi, K., 2003. The origin and evolution of Archean lithospheric mantle, *Precamb. Res.*, **127**, 19–41.
- Gung, Y., Panning, M. & Romanowicz, B., 2003. Global anisotropy and the thickness of continents, *Nature*, **422**, 707–711.
- Hirth, G. & Kohlstedt, D.L., 1996. Water in the oceanic upper mantle: Implications for rheology, melt extraction and the evolution of the lithosphere, *Earth planet. Sci. Lett.*, **144**, 93–108.
- Hirth, G., Evans, R.L. & Chave, A.D., 2000. Comparison of continental and oceanic mantle electrical conductivity: Is the Archean lithosphere dry? *Geochem. Geophys. Geosyst.*, **1**(12), 1030.
- Jones, A.G., Plomerová, J., Korja, T., Sodoudi, F. & Spakman, W., 2010. Europe from the bottom up: a statistical examination of the central and northern European lithosphere–asthenosphere boundary from comparing seismological and electromagnetic observations, *Lithos*, **120**, 14–29.
- Julià, J., Ammon, C.J., Herrmann, R.B. & Correig, A.M., 2000. Joint inversion of receiver functions and surface-wave dispersion observations, *Geophys. J. Int.*, **143**, 99–112.
- Karato, S. & Jung, H., 1998. Water, partial melting and the origin of the seismic low velocity and high attenuation zone in the upper mantle, *Earth planet. Sci. Lett.*, **157**, 193–207.
- Kawakatsu, H., Kumar, P., Takei, Y., Shinohara, M., Kanazawa, T., Araki, E. & Suyehiro, K., 2009. Seismic evidence for sharp lithosphere–asthenosphere boundaries of oceanic plates, *Science*, **324**, 499–502.
- Kennett, B.L.N., Engdahl, E.R. & Buland, R., 1995. Constraints on seismic velocities in the Earth from traveltimes, *Geophys. J. Int.*, **122**, 108–124.
- Kind, R. & Yuan, X., 2010. Seismic Images of the Biggest Crash on Earth, *Science*, **329**, 1479–1480.
- Komatitsch, D., Ritsema, J. & Tromp, J., 2002. The spectral-element method, beowulf computing, and global seismology, *Science*, **298**, 1737–1742.
- Kumar, P., Yuan, X., Kumar, M.R., Kind, R., Li, X. & Chadha, R.K., 2007. The rapid drift of the Indian tectonic plate, *Nature*, **449**, 894–897.
- Kuskov, O.L., Kronrod, V.A. & Prokofev, A.A., 2011. Thermal Structure and Thickness of the Lithospheric Mantle Underlying the Siberian Craton from the Kraton and Kimberlit Superlong Seismic Profiles, *Izvestiya, Phys. Solid Earth*, **47**, 155–175.
- Kustowski, B., Ekström, G. & Dziewonski, A.M., 2008. Anisotropic shear-wave velocity structure of the Earth's mantle: a global model, *J. geophys. Res.*, **113**, B06306, doi:10.1029/2007JB005169.
- Lebedev, S., Chevrot, S. & van der Hilst, R.D., 2002. The 660-km discontinuity within the subducting NW-Pacific lithospheric slab, *Earth planet. Sci. Lett.*, **205**, 25–35.

- Lebedev, S. & Nolet, G., 2003. Upper mantle beneath southeast Asia from S velocity tomography, *J. geophys. Res.*, **108**, doi:10.1029/2000JB000073.
- Lebedev, S., Chevrot, S. & van der Hilst, R.D., 2003. Correlation between the shear-speed structure and thickness of the mantle transition zone, *Phys. Earth planet. Inter.*, **136**, 25–40.
- Lebedev, S., Nolet, G., Meier, T. & van der Hilst, R.D., 2005. Automated multimode inversion of surface and S waveforms, *Geophys. J. Int.*, **162**, 951–964.
- Lebedev, S., Meier, T. & van der Hilst, R.D., 2006. Asthenospheric flow and origin of volcanism in the Baikal Rift area, *Earth planet. Sci. Lett.*, **249**, 415–424.
- Lebedev, S., Endrun, B., Bischoff, M. & Meier, T., 2007. Layering of seismic anisotropy and the past and present deformation of the lithosphere and asthenosphere beneath Germany, XXIV General Assembly of the IUGG, Perugia, abstract.
- Lebedev, S. & van der Hilst, R.D., 2008. Global upper-mantle tomography with the automated multimode inversion of surface and S-wave forms, *Geophys. J. Int.*, **173**, 505–518.
- Lebedev, S., Boonen, J. & Trampert, J., 2009. Seismic structure of Precambrian lithosphere: New constraints from broad-band surface-wave dispersion, *Lithos* **109**, 96–111.
- Lee, C.T.A., Lenardic, A., Cooper, C.M., Niu, F.L., Levander, A., 2005. The role of chemical boundary layers in regulating the thickness of continental and oceanic thermal boundary layers, *Earth planet. Sci. Lett.*, **230**, 379–395.
- Levshin, A.L., Yanovskaya, T.B., Lander, A.V., Bukchin, B.G., Barmin, M.P., Ratnikova, L.I. & Its, E.N., 1989. *Seismic Surface Waves in a Laterally Inhomogeneous Earth*, ed. Keilis-Borok, V.I., Kluwer, Dordrecht.
- Levshin, A.L., Ritzwoller, M.H. & Resovsky, J.S., 1999. Source effects on surface wave group travel times and group velocity maps, *Phys. Earth planet. Inter.*, **115**, 293–312.
- Li, X., Yuan, X. & Kind, R., 2007. The lithosphere–asthenosphere boundary beneath the western United States, *Geophys. J. Int.*, **170**, 700–710.
- Lin, F.-C., Ritzwoller, M.H. & Snieder, R., 2009. Eikonal Tomography: Surface wave tomography by phase-front tracking across a regional broad-band seismic array, *Geophys. J. Int.*, **177**, 1091–1110.
- Maggi, A., Debayle, E., Priestley, K. & Barruol, G., 2006. Multi-mode surface waveform tomography of the Pacific Ocean: a closer look at lithospheric cooling, *Geophys. J. Int.*, **166**, 1384–1397.
- Meier, T., Dietrich, K., Stockhert, B. & Harjes, H.-P., 2004. One-dimensional models of shear wave velocity for the eastern Mediterranean obtained from the inversion of Rayleigh wave phase velocities and tectonic implications, *Geophys. J. Int.*, **156**, 45–58.
- Miller, M.S. & Eaton, D.W., 2010. Formation of cratonic mantle keels by arc accretion: evidence from S receiver functions, *Geophys. Res. Lett.*, **37**, L18305, doi:10.1029/2010GL044366.
- Muyzert, E. & Snieder, R., 1996. The influence of errors in source parameters on phase velocity measurements of surface waves, *Bull. seism. Soc. Am.*, **86**, 1863–1872.
- Nettles, M. & Dziewonski, A.M., 2008. Radially anisotropic shear velocity structure of the upper mantle globally and beneath North America, *J. geophys. Res.*, **113**, B02303, doi:10.1029/2006JB004819.
- Nolet, G., 1990. Partitioned waveform inversion and two-dimensional structure under the Network of Autonomously Recording Seismographs, *J. geophys. Res.*, **95**, 8499–8512.
- O'Reilly, S.Y. & Griffin, W.L., 2010. The continental lithosphere–asthenosphere boundary: can we sample it? *Lithos*, **120**, 1–13.
- Pasyanos, M.E., 2010. Lithospheric thickness modeled from long-period surface wave dispersion, *Tectonophysics*, **481**, 38–50.
- Pedersen, H.A., 2006. Impacts of non-plane waves on two-station measurements of phase velocities, *Geophys. J. Int.*, **165**, 279–287.
- Pedersen, H.A., Bruneton, M., Maupin, V., SVEKALAPKO Seismic Tomography Working Group, 2006. Lithospheric and sublithospheric anisotropy beneath the Baltic Shield from surface-wave array analysis, *Earth planet. Sci. Lett.*, **244**, 590–605.
- Plomerová, J., Kouba, D. & Babuška, V., 2002. Mapping the lithosphere–asthenosphere boundary through changes in surface-wave anisotropy, *Tectonophysics*, **358**, 175–185.
- Plomerová, J. & Babuška, V., 2010. Long memory of mantle lithosphere fabric—European LAB constrained from seismic anisotropy, *Lithos*, **120**, 131–143.
- Priestley, K. & McKenzie, D., 2006. The thermal structure of the lithosphere from shear wave velocities, *Earth planet. Sci. Lett.*, **244**, 285–301.
- Qin, Y., Capdeville, Y., Maupin, V., Montagner, J.-P., Lebedev, S. & Beucler, E., 2008. SPICE Benchmark for global tomographic methods, *Geophys. J. Int.*, **175**, 598–616.
- Roux, E., Moorkamp, M., Jones, A.G., Bischoff, M., Endrun, B., Lebedev, S. & Meier, T., 2011. Joint inversion of long-period magnetotelluric data and surface-wave dispersion curves for anisotropic structure: application to data from Central Germany, *Geophys. Res. Lett.*, **38**, L05304, doi:10.1029/2010GL046358.
- Rychert, C.A., Fischer, K.M. & Rondenay, S., 2005. A sharp lithosphere–asthenosphere boundary imaged beneath eastern North America, *Nature*, **436**, 542–545.
- Rychert, C.A. & Shearer, P.M., 2009. A global view of the lithosphere–asthenosphere boundary, *Science*, **324**, 495–498.
- Rychert, C.A., Shearer, P.M. & Fischer, K.M., 2010. Scattered wave imaging of the lithosphere–asthenosphere boundary, *Lithos*, **120**, 173–185.
- Shapiro, N.M. & Ritzwoller, M.H., 2002. Monte-Carlo inversion for a global shear-velocity model of the crust and upper mantle, *Geophys. J. Int.*, **151**, 88–105.
- Simons, F.J., van der Hilst, R.D., Montagner, J.-P. & Zielhuis, A., 2002. Multimode Rayleigh wave inversion for heterogeneity and azimuthal anisotropy of the Australian upper mantle, *Geophys. J. Int.*, **151**, 738–754.
- Tanimoto, T. & Prindle, K., 2007. Surface wave analysis with beamforming, *Earth Planets Space*, **59**, 453–458.
- Thybo, H., 2006. The heterogeneous upper mantle low velocity zone, *Tectonophysics*, **416**, 53–79.
- Tesauro, M., Kaban, M.K. & Cloetingh, S., 2008. EuCRUST-07: a new reference model for the European crust, *Geophys. Res. Lett.*, **35**, L05313.
- Tesauro, M., Kaban, M.K. & Cloetingh, S., 2009. A new thermal and rheological model of the European lithosphere, *Tectonophysics*, **476**, 478–495.
- Van der Lee, S. & Nolet, G., 1997. Upper-mantle S-velocity structure of North America, *J. geophys. Res.*, **102**, 22 815–22 838.
- Van Heijst, H.J., Snieder, R. & Nowack, R., 1994. Resolving a low velocity zone with surface-wave data, *Geophys. J. Int.*, **118**, 333–343.
- Visser, K., Lebedev, S., Trampert, J. & Kennett, B.L.N., 2007. Global Love wave overtone measurements, *Geophys. Res. Lett.*, **34**, L03302, doi:10.1029/2006GL028671.
- Visser, K., Trampert, J., Lebedev, S. & Kennett, B.L.N., 2008. Probability of radial anisotropy in the deep mantle, *Earth planet. Sci. Lett.*, **270**, 241–250.
- Wessel, P. & Smith, W.H.F., 1995. New version of the Generic Mapping Tools released, *EOS, Trans. Am. geophys. Un.*, **76**, 329.
- Yang, Y. & Forsyth, D.W., 2006. Rayleigh wave phase velocities, small-scale convection, and azimuthal anisotropy beneath southern California, *J. geophys. Res.*, **111**, B07306, doi:10.1029/2005JB004180.
- Yoshizawa, K. & Kennett, B.L.N., 2002. Non-linear waveform inversion for surface waves with a neighbourhood algorithm—application to multimode dispersion measurements, *Geophys. J. Int.*, **149**, 118–133.
- Yoshizawa, K., Miyake, K. & Yomogida, K., 2010. 3D upper mantle structure beneath Japan and its surrounding region from inter-station dispersion measurements of surface waves, *Phys. Earth planet. Inter.*, **183**, 4–19.
- Yoshizawa, K. & Ekström, G., 2010. Automated multimode phase speed measurements for high-resolution regional-scale tomography: application to North America, *Geophys. J. Int.*, **183**, 1538–1558.
- Yuan, H. & Romanowicz, B., 2010. Lithospheric layering in the North American craton, *Nature*, **466**, 1063–1068.
- Zhang, X., Paulssen, H., Lebedev, S. & Meier, T., 2007. Surface wave tomography of the Gulf of California, *Geophys. Res. Lett.*, **34**, doi:10.1029/2007GL030631.
- Zhang, X., Paulssen, H., Lebedev, S. & Meier, T., 2009. 3D shear velocity structure beneath the Gulf of California from Rayleigh wave dispersion, *Earth planet. Sci. Lett.*, **279**, 255–262.